Journal of Colloid and Interface Science 517 (2018) 40–51

Contents lists available at ScienceDirect

Journal of Colloid and Interface Science

journal homepage: www.elsevier.com/locate/jcis

Regular Article

Reinforced carbon fiber laminates with oriented carbon nanotube epoxy nanocomposites: Magnetic field assisted alignment and cryogenic temperature mechanical properties

Yuxin He [a,b,c,*], Song Yang [a], Hu Liu [c,d], Qian Shao [e], Qiuyu Chen [a], Chang Lu [a], Yuanli Jiang [b], Chuntai Liu [c,*], Zhanhu Guo [d,*]

[a] College of Chemical Engineering and Pharmaceutics, Henan University of Science and Technology, Luoyang, Henan 471023, PR China
[b] Henan Energy and Chemical Industry Group Research Institute Co., Ltd., Zhengzhou, Henan 450001, PR China
[c] National Engineering Research Center for Advanced Polymer Processing Technology, Zhengzhou University, Zhengzhou, Henan 450001, PR China
[d] Integrated Composites Laboratory (ICL), Department of Chemical & Biomolecular Engineering, University of Tennessee, Knoxville, TN 37996, USA
[e] College of Chemical and Environmental Engineering, Shandong University of Science and Technology, Qingdao 266590, PR China

GRAPHICAL ABSTRACT

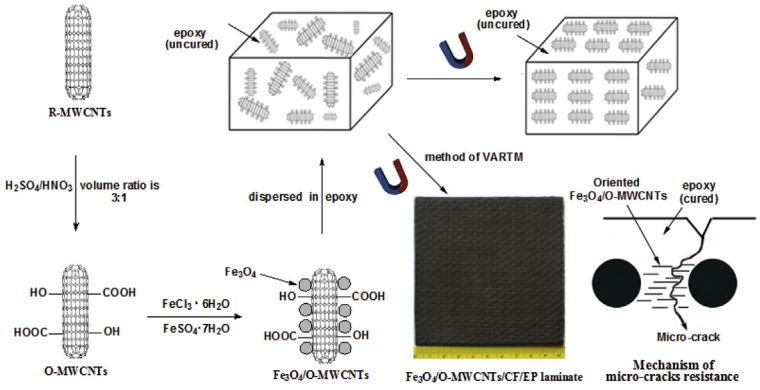

ARTICLE INFO

Article history:
Received 17 November 2017
Revised 11 January 2018
Accepted 24 January 2018

Keywords:
Epoxy
Carbon fiber
Carbon nanotubes
Magnetic field
Oriented
Cryogenic temperature

ABSTRACT

The epoxy nanocomposites with ordered multi-walled carbon nanotubes (MWCNTs) were used to influence the micro-cracks resistance of carbon fiber reinforced epoxy (CF/EP) laminate at 77 K, Oxidized MWCNTs functionalized with Fe_3O_4 (Fe_3O_4/O-MWCNTs) with good magnetic properties were prepared by co-precipitation method and used to modify epoxy (EP) for cryogenic applications. Fe_3O_4/O-MWCNTs reinforced carbon fiber epoxy composites were also prepared through vacuum-assisted resin transfer molding (VARTM). The ordered Fe_3O_4/O-MWCNTs were observed to have effectively improved the mechanical properties of epoxy (EP) matrix at 77 K and reduce the coefficient of thermal expansion (CTE) of EP matrix. The ordered Fe_3O_4/O-MWCNTs also obviously improved the micro-cracks resistance of CF/EP composites at 77 K. Compared to neat EP, the CTE of ordered Fe_3O_4/O-MWCNTs modified CF/EP composites was decreased 37.6%. Compared to CF/EP composites, the micro-cracks density of ordered Fe_3O_4/O-MWCNTs modified CF/EP composites at 77 K was decreased 37.2%.

* Corresponding authors at: College of Chemical Engineering and Pharmaceutics, Henan University of Science and Technology, Luoyang, Henan 471023, PR China (Y.X. He).
E-mail addresses: heyx@haust.edu.cn (Y. He), ctliu@zzu.edu.cn (C. Liu), zguo10@utk.edu (Z. Guo).

https://doi.org/10.1016/j.jcis.2018.01.087
0021-9797/

1. Introduction

Carbon fiber reinforced epoxy resin (CF/EP) laminate, which is fabricated by using epoxy (EP) as matrix and continuous carbon fiber (CF) as reinforcing materials through prepreg, mould pressing and vacuum resin transfer mould (VARTM), has been proved to be one kind of advanced composites due to its superior properties, such as high specific strength and modulus, anti fatigue and corrosion, easy processing, and facile large-scale production. Thus, it is considered to be the most promising structural materials in cryogenic propellant tank for space shuttles [1–6]. When the CF/EP composite tank is used for cryogenic liquid storage and suffers from the process of low-temperature aging and temperature cycling from room temperature (RT) to cryogenic temperature (77 K), micro-cracks will appear and propagate in the composites, causing a variety of defects, such as fiber/matrix interface debonding, pore formation and delamination [7–9]. All these will result in a significant reduction in the performance of composites, leading to the leakage of liquid. Therefore, the CF/EP composites with excellent micro-crack resistance at low temperature are most critical for the design and development of reusable launch vehicles.

Generally, the micro-cracks of CF/EP composites developed during the temperature cycling mainly happen in the resin matrix and mainly arise from different thermal properties between carbon fibers and epoxy resin matrix. For example, the coefficient of thermal expansion (CTE) of epoxy is about $65 \times 10^{-6}\ ^{\circ}C^{-1}$ while about $-12 \times 10^{-6}\ ^{\circ}C^{-1}$ for the carbon fibers [10]. This vast difference will introduce a high internal stress in the composites during the temperature cycle, leading to the formation and growth of micro-cracks in the epoxy matrix. Therefore, the resistance to micro-crack of the CF/EP composites is largely determined by the performance of epoxy matrix, which is closely related to the property and the orientation of the fillers dispersed in the resin except the molecular structure of the epoxy resin.

Previous studies have shown that the micro-crack resistance of CF/EP composites in low temperature environment can be improved by adding fillers, such as alumina, clay, carbon nanotubes (CNTs) and graphene. For example, Timmerman et al. [11] and Khan et al. [12] adopted layered clays as fillers in the fiber-reinforced epoxy composites. The transverse cracking in the symmetric CF/EP composites as a response to cryogenic cycling was significantly reduced and the filler concentration used was much lower than that for the traditional fillers. The particle concentration and their distribution state in the matrix were also observed to be very important in maximizing the benefits of fillers reinforcement. Meanwhile, nanoclays can be easily used to modify the traditional fiber-reinforced composites and enhance their resistance to thermal cycling induced stress. For example, Kim et al. [13] and Yokozeki et al. [14] attempted to enhance the crack resistance of the carbon/epoxy composites by adding multi-walled carbon nanotubes (MWCNTs) into the resin. Due to the embrittlement of the epoxy resin at 77 K, the degree of fracture toughness enhancement obtained from the application of toughened epoxy at cryogenic temperature was less than that at room temperature. The MWCNTs-added carbon/epoxy unidirectional prepregs were fabricated via a filament winding method with different concentrations of MWCNTs (0.0, 0.2 and 0.7 wt%). The material systems blended with 0.2 and 0.7 wt% MWCNTs exhibited an enhanced fracture toughness and low crack density at the cryogenic temperature. The micro-cracks propagated normal to the fibers when viewed along their length through the epoxy matrix beginning at the outer edge of the laminate and ending at 0°/90° ply interface. The results were also reported by Nobelen et al. [15]. In our previous studies, slightly increased mechanical properties and significantly reduced CTE value of epoxy resin were obtained by adding MWCNTs [16]. All the above research results show that the randomly distributed nanofillers can improve the micro-cracks resistance of CF/EP laminates, but the effects of ordered nanofillers in matrix on the mechanical properties of CF/EP laminate at cryogenic temperature have not been reported yet.

Herein, the main purpose of this study is to investigate the effects of functionalized MWCNTs orderly distributed in the matrix on the mechanical properties of CF/EP laminate at 77 K. The optimized formulation of diglycidyl ether of bisphenol-A (DGEBA)/poly oxypropylenediamine (jeffamine D-230) with a low viscosity was selected as the epoxy matrix. Raw MWCNTs (R-MWCNTs), oxidized MWCNTs (O-MWCNTs) and Fe_3O_4/O-MWCNTs were used to modify epoxy. A magnetic induced approach was presented for the preparation of epoxy nanocomposites with Fe_3O_4/O-MWCNTs of ordered alignment. O-MWCNTs were first coated with magnetic Fe_3O_4 particles, and dispersed in epoxy matrix, and finally induced to be aligned by a magnetic force before the suspension was cross-linked. The tensile and impact mechanical properties of the modified epoxy composites at 77 K were studied and compared with those at RT. The mechanisms of CNTs modifiers on the cryogenic toughening and micro-cracks resistance behaviors of modified CF/EP laminates under cryogenic thermal cycling were investigated.

2. Experiments

2.1. Materials

Raw MWCNTs (R-MWCNTs) used in the study were synthesized by catalytic chemical vapor deposition (CM-95, Hanhwa Nanotech, Korea). The epoxy resin was YD-128 (DGEBA, Kukdo Chemical Co. Ltd), which had an epoxide equivalent weight (EEW) of 185-190 eq-1. The curing agent (jeffamine D-230) was provided by New Seoul Chemical Co. Ltd. The reagents used for the acid treatment were nitric acid (60–62%, Junsei Chemical, Japan), and sulfuric acid (95%, Junsei Chemical). Ammonia solution (25%), ethanol (99.5%), iron chloride hexahydrate (99.0%, $FeCl_3{\cdot}6H_2O$), iron sulfate heptahydrate (99.0%, $FeSO_4{\cdot}7H_2O$) and monodispersed magnetite microspheres (99.0%, Fe_3O_4) were purchased from Aladdin regent Co. Ltd, Shanghai, China. All the chemicals and reagents were used without any further treatment. Unidirectional carbon fibers (CARBONEX CF-730, Hankuk Carbon Ltd., Korea) were used as reinforcement for the composites.

2.2. Preparation of O-MWCNTs and Fe_3O_4/O-MWCNTs

Oxidization of MWCNTs (O-MWCNTs): Certain amount of R-MWCNTs was weighed and transferred into a 500 mL flask, then mixed with acid (volume ratio of sulfuric acid and nitric acid was 3:1, carefully added along the wall of the flask). The mixture was heated to 110 °C under strong magnetic stirring and then maintained at this temperature for an additional hour. The O-MWCNTs were separated by using cellulose acetate membrane and repeatedly washed with distilled water until the pH value was 7. Finally, the collected O-MWCNTs were dried in a vacuum oven at 60 °C.

Fe_3O_4/O-MWCNTs: The Fe_3O_4/O-MWCNTs were synthesized by an in-situ chemical oxidation and co-precipitation method, which was slightly modified from the reported method [17]. Briefly, 40 mg O-MWCNTs were dispersed ultrasonically with 150 mL DI water in the flask for one hour. Then, the flask was purged with N_2 for 30 min. A solution of $FeCl_3{\cdot}6H_2O$ (48.0 mg) and $FeSO_4{\cdot}7H_2O$ (247.1 mg) in DI water (50 mL) was purged with N_2 for 30 min and then added to the flask. The flask was transferred to a water bath at

30 °C under continuous agitation. Ammonia solution (25%) was added continuously until the pH of the system reached 12 during the stirring process. The final mixture was stirred for an additional 10 min and then kept in a water bath at 65 °C for 2 h. Finally, the mixture was washed thoroughly with water to neutral pH and dried under vacuum at room temperature. The preparation of O-MWCNTs and Fe_3O_4/O-MWCNTs was schematically shown in Fig. 1a.

2.3. Preparation of MWCNTs/epoxy composites and carbon fiber reinforced epoxy laminate

MWCNTs/epoxy composites: Certain amount of R-MWCNTs (O-MWCNTs or Fe_3O_4/O-MWCNTs) was mixed with the epoxy resin using a vacuum mixer (ARV-310, Thinky Corporation, Japan) for 5 min, and the mixture was sonicated for 30 min. Then, the curing agent D-230 in the ratio of 100:30 to epoxy by weight was added under vigorous mechanical stirring to achieve a homogeneous system. The resultant mixture was cast into a silicone mould and cured at room temperature. Finally, the sample was post-cured in an oven at 125 °C for 3 h. As for the Fe_3O_4/O-MWCNTs modified epoxy composites, a constant magnetic field of 0.7 T was applied (Fig. 1b) during the curing process to achieve an ordered dispersion of Fe_3O_4/O-MWCNTs.

Carbon fiber reinforced epoxy laminate: The carbon fiber reinforced epoxy laminates with dimensions of about 15.24 × 15.24 c m^2 were prepared by the vacuum-assisted resin transfer molding (VARTM) technique. Before crosslinking, the sample was also placed into a constant magnetic field of 0.7 T at room temperature until it cross-linked. Finally, the laminates were put into an oven at 125 °C for 3-h post-curing. The symmetric laminates consisted of nine plies of carbon fabric in a $[0°_3, 90°_3]_s$ configuration. Fig. 1c shows the scheme for the preparation of Fe_3O_4/O-MWCNTs/CF/EP laminate (left) and photograph of Fe_3O_4/O-MWCNTs/CF/EP laminate (right).

2.4. Characterizations

Fourier transform infrared (FTIR) spectra were recorded with a FTIR analyzer (model 6700; Nicolet, Madison, Wisconsin, USA), which was operated from 500 to 4000 cm^{-1} at room temperature. X-ray diffractometer (XRD) of D8-Advance supplied by Germany was used to scan the specimens from 20° to 70° at a rate of 2° per min. Cu K_α radiation (λ = 1.5406 Å), the X-ray source, was generated at the voltage of 40 kV and a current of 40 mA. X-ray photoelectron spectroscopy (XPS) analysis was carried out in an ultra high vacuum system equipped with a Kratos AXIS Ultra hemispherical electron analyzer, using a monochromatic Al K_α source (1486.6 eV), at a base pressure of 2×10^{-10} mbar. Magnetic characterization of the samples was performed via vibrating sample magnetometer (VSM Lakeshore, Model 7400 series) with an applied field of -5000 Oe $\leq H \leq$ 5000 Oe. The field emission scanning electron microscopy (FE-SEM) images were obtained with the JEOL JSM-6701F type. Prior to examination, the fracture surfaces

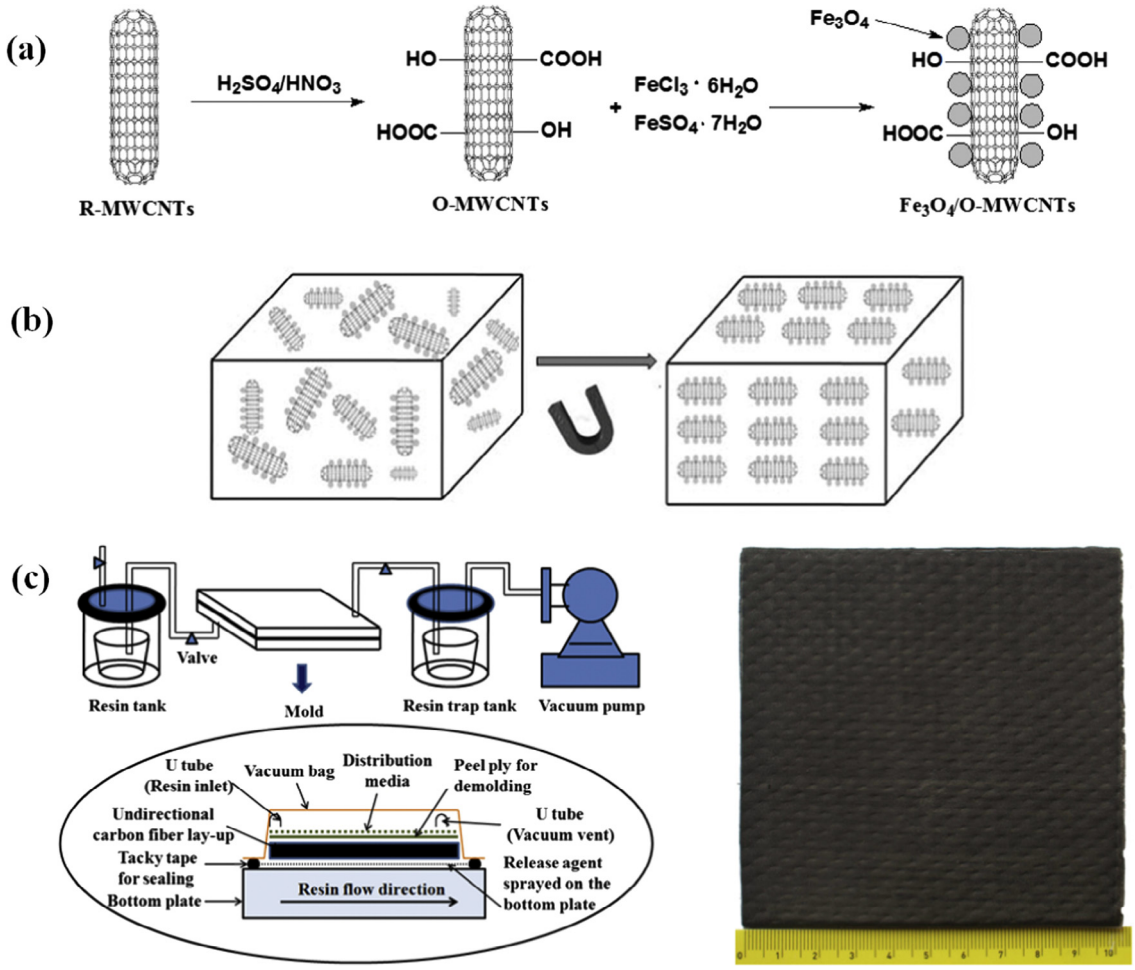

Fig.1. (a) Scheme for preparation of O-MWCNTs and Fe_3O_4/O-MWCNTs, (b) schematic diagram of the preparation of ordered Fe_3O_4/O-MWCNTs modified epoxy composites, (c) scheme for preparation of Fe_3O_4/O-MWCNTs/CF/EP laminate (left) and photograph of Fe_3O_4/O-MWCNTs/CF/EP laminate (right).

were cleaned using alcohol and were then coated with a thin evaporated layer of gold to improve conductivity. The transmission electron microscopy (TEM) images were taken on a JEOL JEM 2200FS under a working voltage of 200 kV. The thermal expansions of the neat epoxy and the CNTs modified epoxies were tested using a TA instrument TMA Q 400 at a heating rate of 10 °C min^{-1} from −150 to 150 °C and a preload force of 0.5 N.

The tensile samples were prepared according to the recommendation of ASTM D638-99. In this study, MTS Landmark Servohydraulic Test System was used to set up the cryogenic tensile test. The environmental chamber of this test system can be cooled down to −150 °C by evaporating the cryogenic liquid medium.

The impact properties of the CNTs/epoxy composites were tested using notched Izod impact testing according to the ASTM D-256 specification. The specimens for impact testing were immersed in liquid nitrogen at 77 K for over 15 min before being mounted onto the impact tester. The pendulum of the impact tester was released immediately against the notch after the specimen was mounted onto the impact tester and each impact test was completed in a couple of seconds to avoid the change of temperature inside the specimens. At least five specimens were tested for each blend.

In order to check the micro-cracks in the carbon fiber reinforced epoxy composite laminates, the samples were allowed to equilibrate at 22 °C and then placed in a liquid nitrogen bath (77 K) for 10 min. After exposure to liquid nitrogen, the samples were placed inside a desiccators and allowed to return to room temperature. Each sample was exposed to a minimum of five thermal cycles until optical microscope revealed no micro-cracks. Three specimens from each laminate were cycled at cryogenic temperature. Each sample was examined prior to cycling to ensure no initial cracks or defects on the surface. After each material had reached thermal equilibrium in a desiccator, it was examined at ×160 magnification using an optical microscope. Optical photomicrographs were taken to document the sample response and the number of micro-cracks on the polished surface was counted.

3. Results and discussion

3.1. Magnetic nanofillers

Fig. 2a shows the FT-IR spectra of MWCNTs, O-MWCNTs, Fe_3O_4/O-MWCNTs, and Fe_3O_4. The 3440 and 1048 cm^{-1} bands are attributed to the presence of —OH, and the 1634 cm^{-1} band is due to the presence of C=C on the surface of the R-MWCNTs (Fig. 2a), which results from either ambient atmospheric moisture or oxidation during purification of raw materials [18]. In addition, two new bands of O-MWCNTs appeared at 1716 and 1165 cm^{-1}, corresponding to the C=O and C—O stretching vibrations of the carboxylic groups (—COOH), respectively. The absorption peak at 3440 cm^{-1} is observed for the —OH functionality and the peak at 1382 cm^{-1} is due to the —OH bending deformation in —COOH. All these observations indicate that the MWCNTs have been functionalized by oxidation and hence the formation of —OH and —COOH groups on O-MWCNTs [19]. In comparison to O-MWCNTs, the spectrum of Fe_3O_4/O-MWCNTs shows an extra peak which belongs to Fe_3O_4. The peak at 570 cm^{-1} for Fe_3O_4/O-MWCNTs is due to the Fe-O stretching mode of the tetrahedral site in Fe_3O_4 [20,21].

Fig. 2b displays the XRD patterns of O-MWCNTs, Fe_3O_4/O-MWCNTs and pure Fe_3O_4 particles. It can be seen that both the XRD curves for O-MWCNTs and Fe_3O_4/O-MWCNTs display the (0 0 2) diffraction peak of hexagonal graphite, indicating that the graphite structure of the O-MWCNTs support was not destroyed by the acidic treatment and the particles preparation [22]. Six new peaks at 30.11°, 35.51°, 43.11°, 53.41°, 56.91° and 62.41° are observed, while the characteristic peak of O-MWCNTs remains unchanged. The positions and relative intensities of these non-CNTs related new peaks match well with the (2 2 0), (3 1 1), (4 0 0), (4 2 2), (5 1 1), and (4 4 0) planes of the standard XRD data for the cubic spinal crystal structure of Fe_3O_4 [23]. No peaks corresponding to impurities are detected. Thus, it could be concluded that Fe_3O_4/O-MWCNTs particles were formed during the decomposition process.

The surface composition and chemical state of Fe on the Fe_3O_4/O-MWCNTs were further analyzed by XPS. Fig. 2c shows the typical spectra for Fe_3O_4/O-MWCNTs. All the binding energies are referenced to C 1s at 284.6 Ev [24]. As expected, distinct C 1s, O 1s and Fe 2p peaks are observed in the survey scan spectrum of the Fe_3O_4/O-MWCNTs sample. The typical Fe 2p XPS narrow scan spectrum presents two main peaks at about 711.2 and 725 eV corresponding to the spin–orbit split doublet of Fe 2p 3/2 and Fe 2p 1/2, respectively, which could be identified as the Fe_3O_4 entity [25].

Fig. 2d shows the magnetic properties of pure Fe_3O_4 and Fe_3O_4/O-MWCNTs particles investigated at room temperature. The Fe_3O_4 and Fe_3O_4/O-MWCNTs particles are observed to exhibit a superparamagnetic behavior without remanence and coercivity, which may be related to the small size of these Fe_3O_4 particles [26,27]. The saturation magnetization value of Fe_3O_4/O-MWCNTs reached 48.56 emu/g, which was lower than that of pure Fe_3O_4 particles (70.94 emu/g) [28]. This decrease can be attributed to the existence of O-MWCNTs. The inserted photo in Fig. 2d shows the stability of Fe_3O_4/O-MWCNTs dispersed in ethanol and the dispersion retains its homogeneous state for at least 2 weeks at room temperature (Insert photo left). The Fe_3O_4/O-MWCNTs could be quickly separated from their dispersion by holding the sample close to a commercial magnet (Insert photo right), indicating that it is possible to manipulate the Fe_3O_4/O-MWCNTs by an external magnetic field.

Fig. 3 presents the SEM and TEM images of R-MWCNTs, O-MWCNTs and Fe_3O_4/O-MWCNTs. It can be seen clearly that R-MWCNTs are curled and entangled with each other (Fig. 3a). After the acid treatment, big agglomerations were found due to the large polar forces derived from the strong interactions among these polar groups on their surface of MWCNTs [16,29], and the interspaces in O-MWCNTs also become smaller [30]. From Fig. 3c–e, several distinctive characteristics for Fe_3O_4/O-MWCNTs are observed. First, most O-MWCNTs have been coated with magnetite microspheres. Second, the distribution of Fe_3O_4 on the O-MWCNTs surface is relatively uniform. Besides, the overall tubular structure of CNTs remains intact after surface reactions. From TEM images (Fig. 3d and e), it can be seen that Fe_3O_4 particles on O-MWCNTs surface were distributed with irregular shape and slight aggregation, which might be due to a relatively high surface energy of small sized Fe_3O_4 particles. The average size of Fe_3O_4 particles is about 12.4 nm. The d-space of Fe_3O_4 particles is 0.175 nm (Fig. 3f).

3.2. Epoxy nanocomposites

The stress-strain curves of neat epoxy, R-MWCNTs, O-MWCNTs and ordered Fe_3O_4/O-MWCNTs modified epoxy composites (filler content was 0.5 wt%) at 77 K and RT are shown in Fig. 4. Clearly, the failure strain of modified epoxy composites at both RT and 77 K was observed to be significantly improved as compared with that of neat epoxy. All the CNTs/epoxy composites exhibit relatively ductile behaviors at room temperature compared to that at 77 K. The mechanical properties of neat epoxy, O-MWCNTs modified epoxy composites and Fe_3O_4/O-MWCNTs modified epoxy composites (ordered) at both 77 K and RT are summarized in Table 1. The error bars denote the standard deviation for the impact strength.

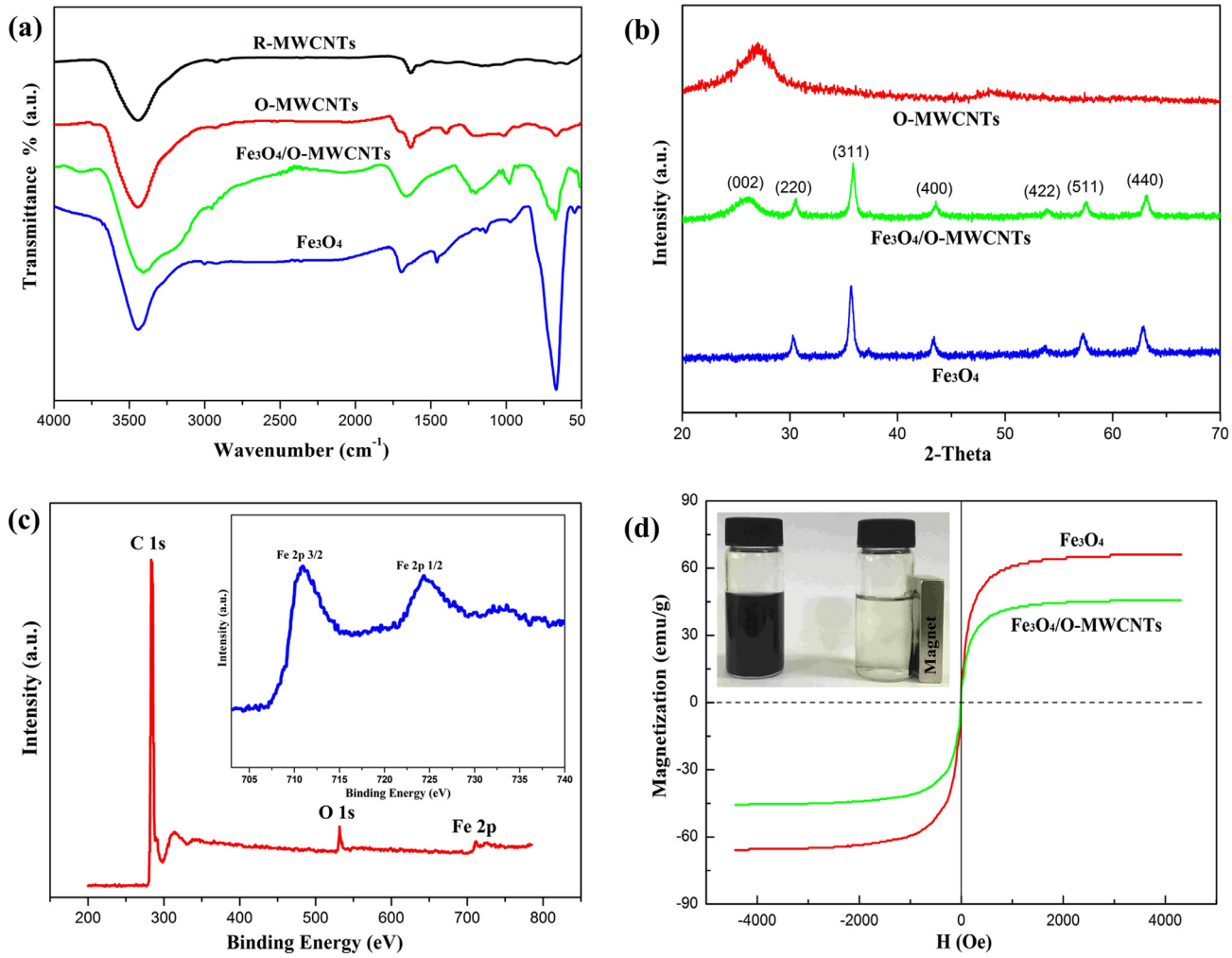

Fig. 2. (a) FT-IR spectra of MWCNTs, O-MWCNTs, Fe_3O_4/O-MWCNTs, and Fe_3O_4. (b) XRD patterns of O-MWCNTs, Fe_3O_4/O-MWCNTs and pure Fe_3O_4 particles. (c) XPS spectra of Fe_3O_4/O-MWCNTs. (d) Magnetization curves at 300 K of pure Fe_3O_4 and Fe_3O_4/O-MWCNTs (Insert photo: An aqueous suspension of Fe_3O_4/O-MWCNTs before (left) and after placing near a magnet (right)).

From Table 1, it can be seen that the introduction of nanoparticles into epoxy resin can effectively enhance the mechanical properties of the cured epoxy resin at RT and 77 K. Different enhancements were observed due to different CNTs/epoxy interfacial bonding and the dispersion state of CNTs in the epoxy matrix. R-MWCNTs could be easily pulled out from the epoxy matrix because of poor interfacial bonding between R-MWCNTs and epoxy matrix. The relatively weak bonding led to poor stress transfer from weaker epoxy matrix to stronger R-MWCNTs and the R-MWCNTs would have a low reinforcing efficiency. After oxidation, the —OH and —COOH groups were introduced on the surface of MWCNTs, which could form covalent bonding with epoxy matrix. Compared to neat epoxy, the tensile strength of O-MWCNTs/epoxy composites at RT was increased from 68.7 to 71.5 MPa, an increase of 4%. Under the external magnet field, the Fe_3O_4/O-MWCNTs were orderly arranged in the epoxy matrix. The better interfacial bonding between Fe_3O_4/O-MWCNTs and epoxy matrix than R-MWCNTs and O-MWCNTs led to a better stress transfer from epoxy to CNTs. When the arranged direction of Fe_3O_4/O-MWCNTs was perpendicular to the direction of the force applied in the sample, Fe_3O_4/O-MWCNTs could play a good role in preventing the growth of micro-cracks in the epoxy matrix. Compared with neat epoxy, the tensile strength of Fe_3O_4/O-MWCNTs/epoxy (ordered) composites at RT was increased from 68.7 to 74.4 MPa, an increase of 8.3%. The effects of Fe_3O_4/O-MWCNTs on the tensile properties of epoxy resin at RT is similar to the epoxy nanocomposites filled with protruding nanoparticles on the graphene nanosheets [31–33].

From Table 1, it can be seen that the tensile strength of epoxy composites contained Fe_3O_4/O-MWCNTs, which had been induced by magnetic field, was better than that of the epoxy composites contained disordered fillers (R-MWCNTs and O-MWCNTs) at 77 K. Compared with neat epoxy, R-MWCNTs/epoxy and O-MWCNTs/epoxy, the tensile strength of Fe_3O_4/O-MWCNTs/epoxy (ordered) composites at 77 K was increased from 81.6, 87.2 and 89.5 MPa to 93.5 MPa, a rising scope of 14.6%, 7.2% and 4.5%. This may be due to the oriented Fe_3O_4/O-MWCNTs, which increased the interfacial area and could effectively prevent the matrix cracks extend along the force direction. In addition, the tensile strength of each sample at 77 K is larger than that at RT, which can be explained by the following reasons. Firstly, when the temperature decreases from RT to 77 K, the chemical bond and molecules of epoxy matrix will shrink and the binding forces between molecules will become stronger and the interfacial chemical bonds between epoxy and functionalized CNTs also become stronger [34]. Thus, a larger load will be needed to break the epoxy matrix at 77 K, leading to a higher strength of the epoxy matrix at 77 K than that at RT [16]. Secondly, the thermal contraction of epoxy matrix due to the decrease of

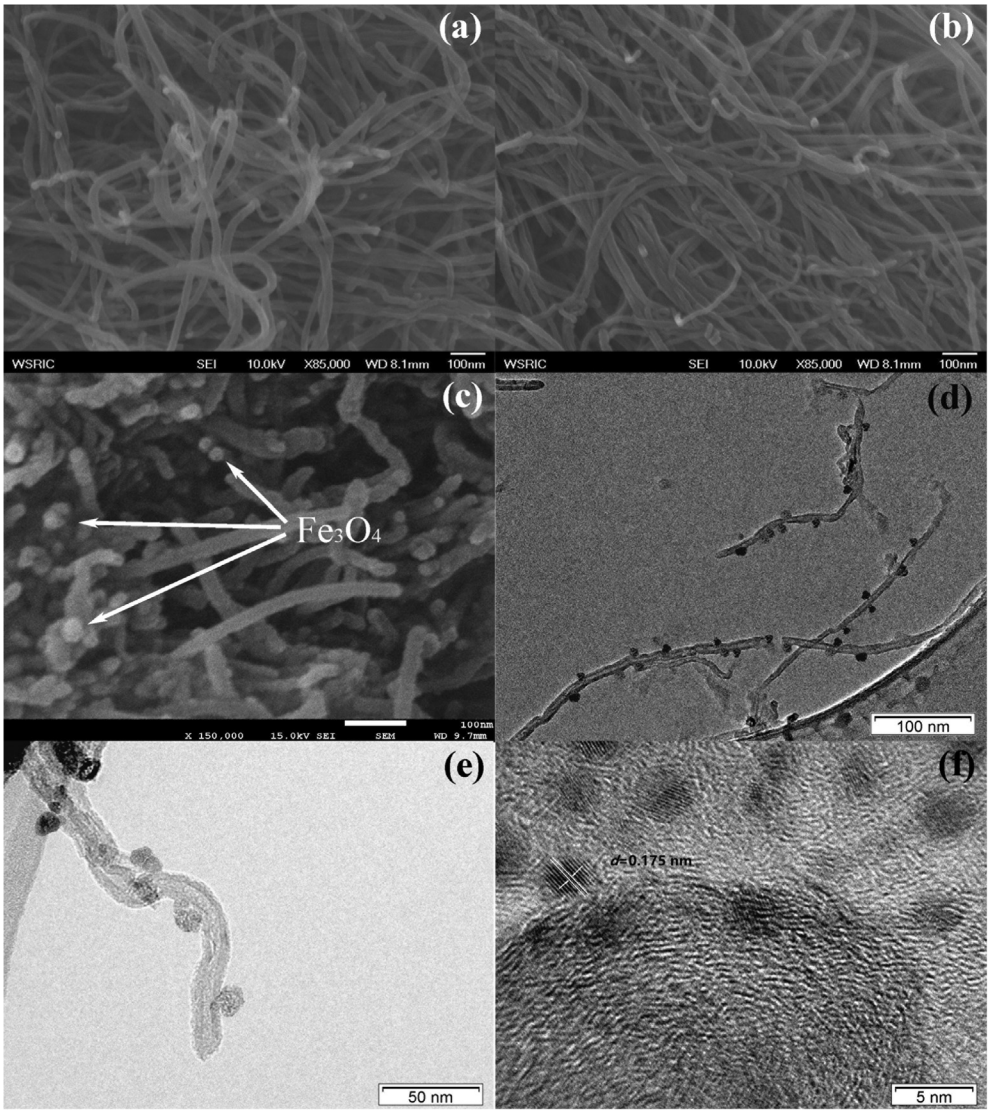

Fig. 3. SEM images of MWCNTs (a), O-MWCNTs (b) and Fe_3O_4/O-MWCNTs (c), TEM image of Fe_3O_4/O-MWCNTs (d, e, and f).

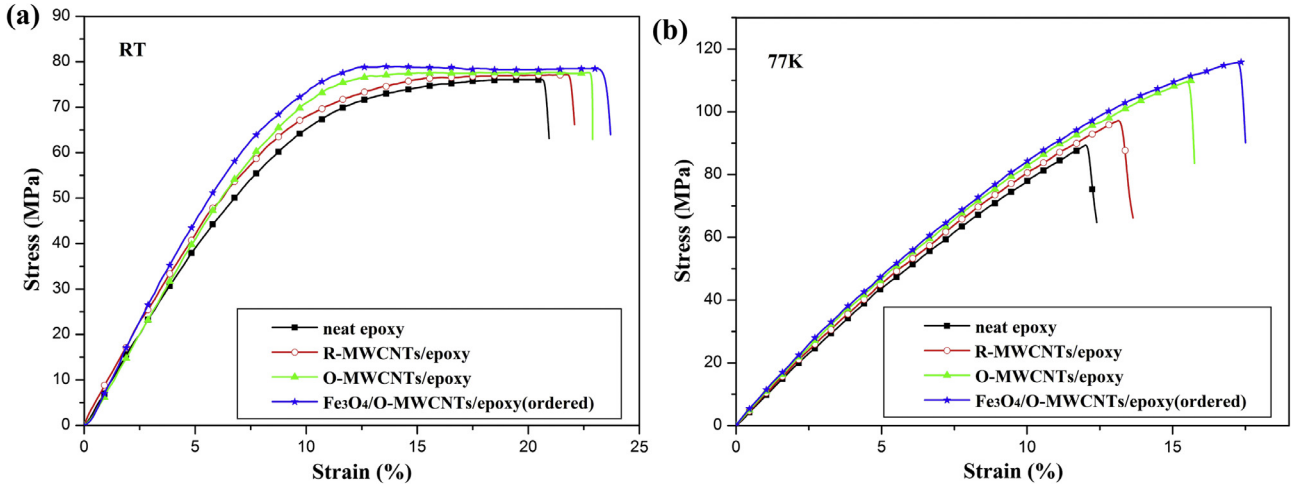

Fig. 4. Stress-strain curves of neat epoxy, R-MWCNTs and O-MWCNTs modified epoxy composites and Fe_3O_4/O-MWCNTs modified epoxy composites (ordered) at (a) RT and (b) 77 K.

Table 1
Mechanical properties of epoxy matrix and modified epoxy composites.

Sample	Filler content (wt.%)	Tensile strength (MPa)		Young's modulus (GPa)		Impact strength (MPa)	
		77 K	RT	77 K	RT	77 K	RT
Neat epoxy	0	81.6 ± 3.2	68.7 ± 2.1	4.5 ± 4.0	2.6 ± 0.1	36.5 ± 2.6	54.2 ± 2.3
R-MWCNTs/epoxy	0.5	87.2 ± 1.6	70.1 ± 1.7	4.7 ± 2.1	2.8 ± 0.1	38.1 ± 4.3	57.7 ± 3.1
O-MWCNTs/epoxy	0.5	89.5 ± 2.5	71.5 ± 1.1	4.8 ± 1.8	3.1 ± 0.2	38.5 ± 3.3	63.9 ± 1.7
Fe_3O_4/O-MWCNTs/epoxy(ordered)	0.5	93.5 ± 1.8	74.4 ± 1.3	5.4 ± 2.7	3.5 ± 0.1	40.2 ± 2.5	69.2 ± 2.9

temperature increased the clamping stress. (The coefficient of thermal expansion of epoxy resin is much higher than CNTs. With the temperature decreased from RT to 77 K, the molecules of epoxy resin shrink and is tightly entwined on CNTs.) to the CNTs at 77 K, which would lead to a stronger interfacial bonding between CNTs and epoxy. This phenomenon has also been reported in our previous work [18].

Table 1 also displays that the Young's modulus of CNTs/epoxy composites at both 77 K and RT increased, consistent with the increased interfacial interaction between CNTs and epoxy matrix. The Young's modulus was increased respectively by 4.5%, 6.7% and 20.0% at 77 K, and 7.7%, 19.2% and 34.6% at RT compared with that of the neat epoxy (4.5 GPa at 77 K and 2.6 GPa at RT). Besides, the Young's modulus at 77 K was higher than that at RT for each sample. On one hand, the molecules of the epoxy matrix became stiffer due to the restrained mobility of the molecules when the temperature decreased from RT to 77 K [34]. On the other hand, any material would become stiffer at cryogenic temperatures and thus the MWCNTs would also become stiffer at 77 K than at RT [34]. As a result, in terms of the theories for particulate polymer composites [35] or short fibers reinforced polymer composites, it can be easily inferred that the Young's modulus of the CNTs/epoxy composites must be higher at 77 K than that at RT.

From Table 1, the impact strength of R-MWCNTs, O-MWCNTs and Fe_3O_4/O-MWCNTs modified epoxy resin was also observed to be greatly enhanced by 4.3%, 5.4% and 10.1% at 77 K and 6.4%, 17.8% and 27.7% at RT, respectively. This can be explained using the selective dispersion of different MWCNTs in the brittle DGEBA phase. In terms of the synthetic sequence, CNTs were first mixed with DGEBA and the resulting mixture was then blended with curing agent, so the brittle DGEBA phase could be effectively toughened by the introduction of R-MWCNTs. As for the addition of functionalized MWCNTs, covalent bonding was formed between functionalized MWCNTs and epoxy matrix, leading to a higher impact strength. Thus, compared with neat epoxy (36.5 MPa at 77 K and 54.2 MPa at RT), the impact strength (38.5 MPa at 77 K and 63.9 MPa at RT) of O-MWCNTs/epoxy was increased both at 77 K and RT. Besides, it can also be seen that the impact strength (40.2 MPa at 77 K and 69.2 MPa at RT) of epoxy composites contained Fe_3O_4/O-MWCNTs was better than that of the epoxy composites contained disordered fillers both at 77 K and RT. This may be due to the oriented Fe_3O_4/O-MWCNTs, which play the role of preventing the micro-cracks extend along the vertical force direction [36].

From Table 1, it can be seen that the Fe_3O_4/O-MWCNTs modified epoxy resin has the best mechanical performance when the content of filler is 0.5 wt%. It may be due to the fact that the Fe_3O_4/O-MWCNTs can be dispersed uniformly in the epoxy matrix and play a role in reinforcing the polymer matrix. Even if Fe_3O_4 particles were loaded on the surface of O-MWCNTs after the modification, a large number of —OH, —COOH and other functional groups on the Fe_3O_4/O-MWCNTs surface can form the covalent bond C—O—C with epoxy matrix and form a strong interface interaction. This strong interaction can transfer the load from the weak epoxy matrix to the strong fillers under an external force load. The addition of CNTs can improve the toughness of the epoxy composites, which may be related to the structure of the CNTs itself. The CNTs can be viewed as a coaxial structure with a number of single walled carbon nanotubes (SWCNTs) with different diameters, which have concentric structures and are held together by Van der Waals force. The outer wall of the CNTs in the epoxy composites is functionalized, which can afford the load, but the inner wall does not afford the load. When the epoxy composite is loaded with an external force, the outer wall of the Fe_3O_4/O-MWCNTs is partially exfoliated and removed due to the acid treatment, so that the inner tube is pulled out, which can cause the failure of the Fe_3O_4/O-MWCNTs, thus improving the toughness of the epoxy composites.

Fig. 5 shows the SEM images with a relatively low magnification of the fracture surface of epoxy based composites contained different fillers after the impact testing at 77 K and at RT. The fracture surfaces of neat epoxy resins at 77 K (Fig. 5a) and RT (Fig. 5b) were smooth with some "wavelike" patterns, which were caused by rapid crack propagations [4,37]. Meanwhile, the fracture surfaces of EP composites with different types of CNTs became rougher than that of neat epoxy, and lots of micro-crack were also observed, all these were ascribed to good interaction between CNT and epoxy and the resistance of CNTs to the propagation of micro-cracks (Fig. 5c–h).

In order to get an insight into the details of the fracture surfaces at 77 K, the SEM images with a relatively high magnification were taken as shown in Fig. 6. It can be seen that the fracture surface of neat epoxy resins at 77 K (Fig. 6a) was smooth. The R-MWCNTs reinforced epoxy composites showed a layered rougher surface rather than a smooth plane like the neat resin at 77 K (Fig. 6b). The curled rich resin area and protruding tubes suggested non-uniform dispersion and weak bonding. It can be seen that some O-MWCNTs were impregnated in the epoxy resin and some were partially pulled out of the epoxy (Fig. 6c). From Fig. 6d, one end of Fe_3O_4/O-MWCNTs was observed to be embedded in the epoxy resin and the other end was exposed to the outside, which were induced by external magnetic field to align the magnetic fillers in the epoxy resin. The aligning direction of Fe_3O_4/O-MWCNTs was perpendicular to the direction of impact force. In comparison, all CNTs modified epoxy samples showed a much rougher, heavily layered fracture surface, and more uniformly dispersed CNTs networks. The multilayered rough fracture face suggests that micrometer sized crack propagations were effectively prevented owing to the improved dispersion and interface bonding; otherwise, continuous crack propagations would produce relatively smooth "wavelike" patterns [38].

The coefficient of thermal expansion (CTE) quantifies the thermal expansion of the solid. The coefficient can be volumetric or linear according to whether the measurement is determined by the change of the volume or length of the sample. For polymers such as epoxy resin, the CTE values can be divided into two parts: below and above the glass-transition temperature (T_g). The most useful CTE concerns the temperature below T_g, since polymers or composites lose most of their mechanical properties above T_g. The CTE of the samples can be calculated based on the dimension change curves as shown in Fig. 7a. Fig. 7b shows the CET values of the samples below T_g. From Fig. 7b, it can be known that the CTE values of

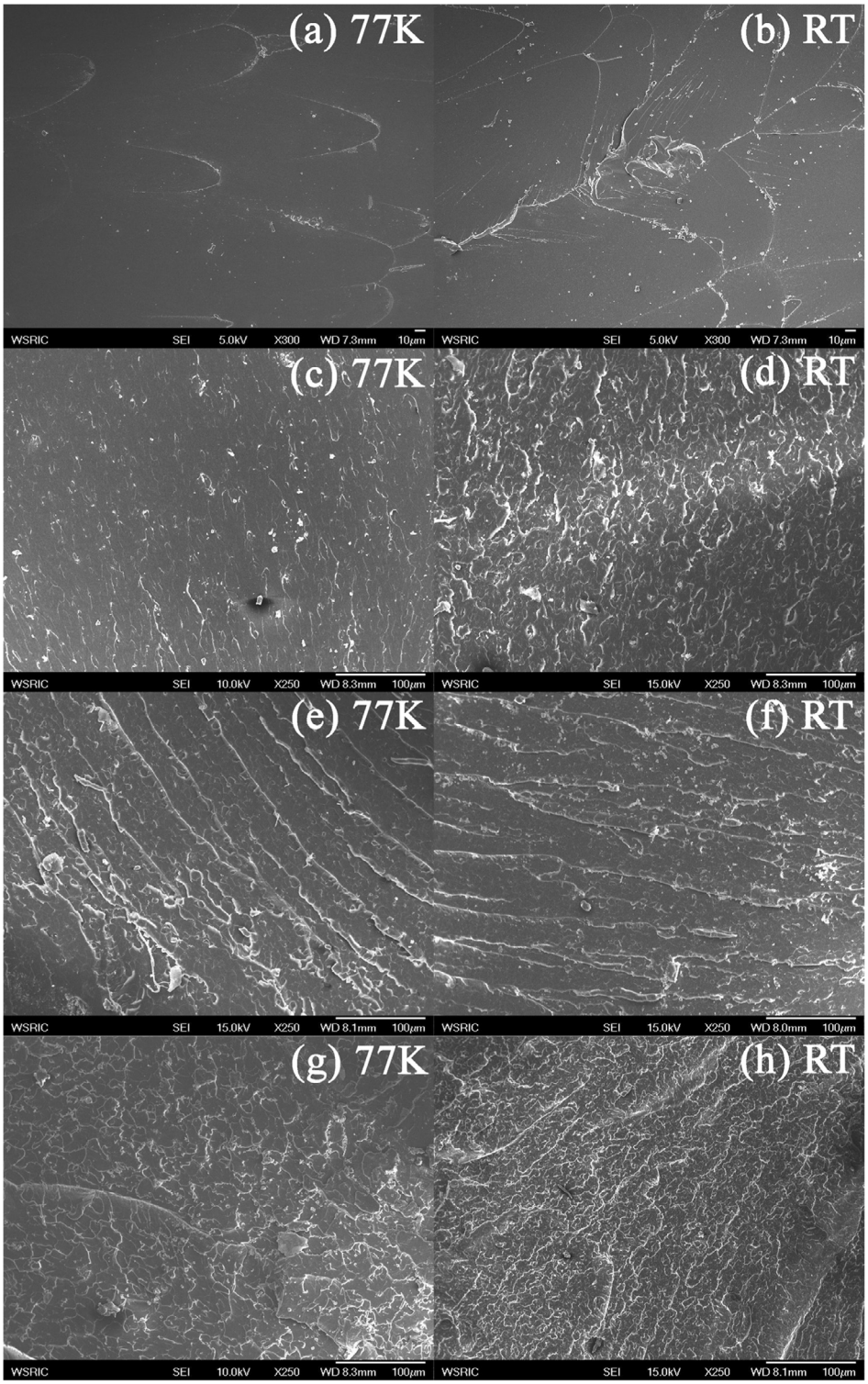

Fig. 5. SEM images with a relatively low magnification of the fracture surface of epoxy based composites after impact testing at 77 K and at RT: (a–b) the neat epoxy, (c–d) containing 0.5% R-MWCNTs, (e–f) containing 0.5% O-MWCNTs and (g–h) containing 0.5% Fe_3O_4/O-MWCNTs (ordered).

the modified epoxies are lower than that of the neat epoxy. In comparison with neat epoxy, the R-MWCNTs, O-MWCNTs and Fe_3O_4/O-MWCNTs modified epoxies show CTE reductions of 19.7%, 28.7% and 37.6%, respectively. The magnitude of the CTE depends on the structure of materials. For single-phase materials, the CTE is determined by the atomic bonding, molecular structure, and molecular assembly [38]. An elevated temperature would increase the thermal energy and led to an increase in the atomic movement. A weaker atomic bonding owing to the increased inter-atomic distance would give a larger CTE value [38,39]. For multiphase materials, such as composites, the CTE is dependent on each component phase and also on the interactions between each phase. However, a weak interfacial bonding between phases could not effectively incorporate the contributions of each component, while a strong

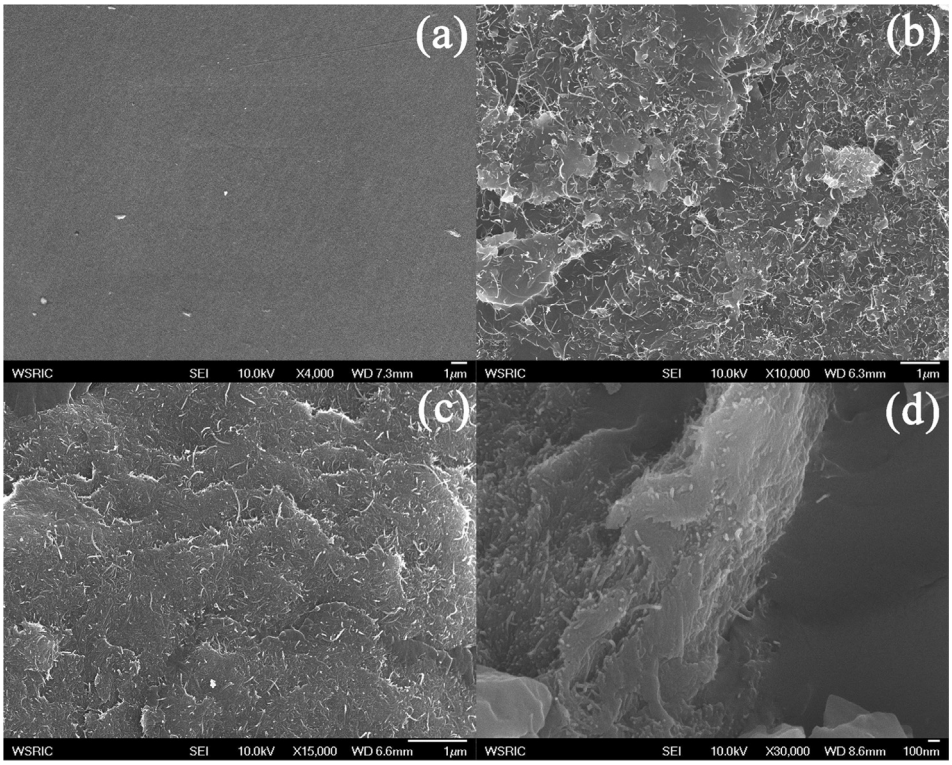

Fig.6. SEM images with a relatively high magnification of the fracture surface of epoxy based composites after impact testing at 77 K: (a) the neat epoxy, (b) containing 0.5% R-MWCNTs, (c) containing 0.5% O-MWCNTs, (d) containing 0.5% Fe_3O_4/O-MWCNTs (ordered).

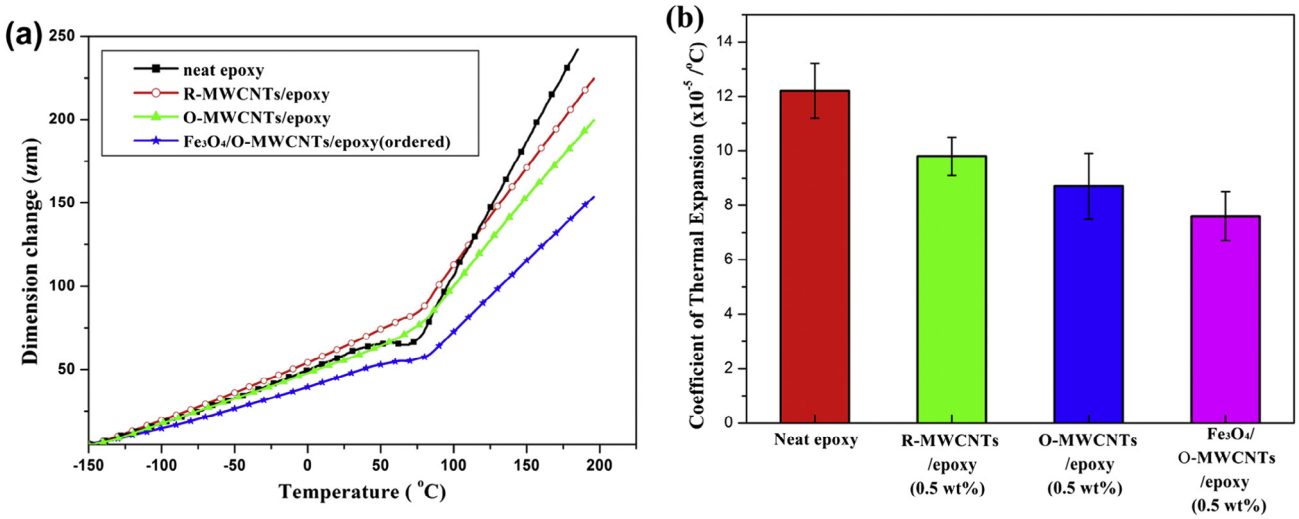

Fig. 7. (a) Variation of thermal expansion of neat epoxy and the modified epoxies with temperature, (b) CTE values of neat epoxy and the modified epoxies below T_g.

interfacial bonding can reduce the thermal-expansion properties significantly [40,41]. Therefore, an inspection of the reduction in CTE values of the modified epoxies suggests that O-MWCNTs and Fe_3O_4/O-MWCNTs can effectively enhance the micro-cracks behavior of the carbon fiber reinforced epoxy composites (under cryogenic thermal cycling) for cryogenic applications. Compared with neat epoxy, the CTE value of Fe_3O_4/O-MWCNTs modified epoxy composite was largely reduced, because of the Fe_3O_4/O-MWCNTs aligned in the epoxy matrix. It is proved that the ordered arrangement of CNTs with two-dimensional structure can further reduce the CTE value of epoxy resin and increase the thermal properties at 77 K.

3.3. Laminate microcracking

The CF/EP laminates prepared by VARTM were used to study the micro-cracks morphology and to determine the crack density. The optical photomicrographs of the micro-cracks morphologies developed as a result of cryogenic cycling are shown in Fig. 8. The micro-cracks propagate normal to the carbon fibers along their length, beginning at the outer edge of the laminates and ending at the 0°/90° ply interface. It is seen that the micro-cracks did not appear to change with the MWCNTs type. It can also be noted that the micro-crack is formed in the outer side of the laminate. This phenomenon has been noted in previous work and may be attributed

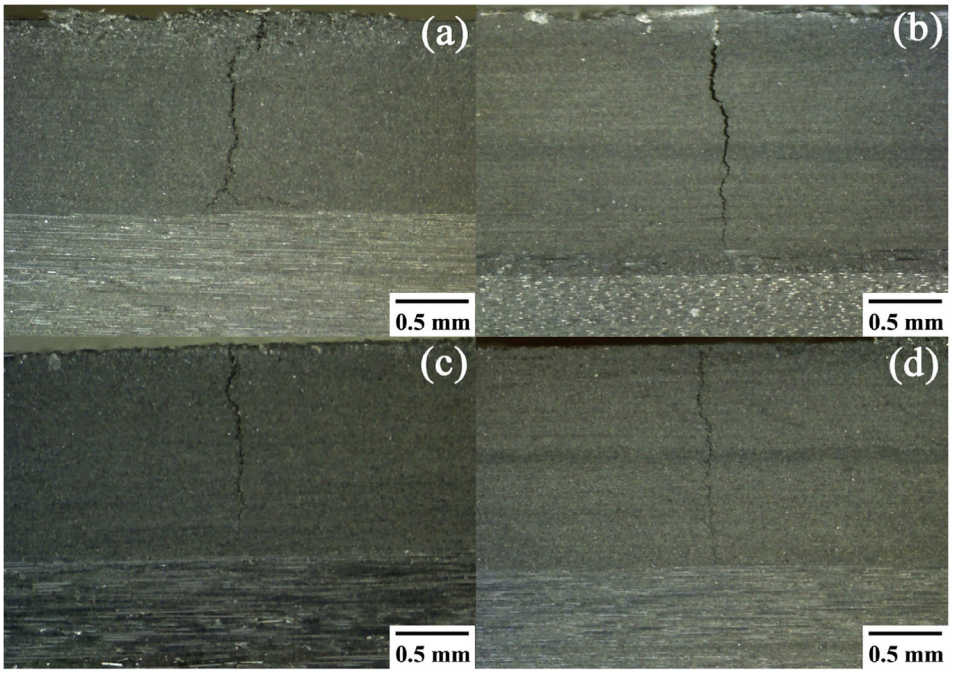

Fig. 8. Reflected optical micrographs of cryogenically cycled carbon fiber/epoxy laminates: (a) CF/EP laminate, (b) R-MWCNTs modified CF/EP laminate, (c) O-MWCNTs modified CF/EP laminate and (d) Fe_3O_4/O-MWCNTs modified CF/EP laminate.

to the roughness of the vacuum back side, which might have contributed more crack initiation sites than the cutting tool side [42,43].

Fig. 9 shows the micro-cracks density in CF/EP laminates filled with different types of MWCNTs. Significant variations in the micro-cracks density are observed. The addition of MWCNTs can effectively improve the micro-cracks resistance of the laminates. This may be due to the reinforcing efficiency of the MWCNTs, which lowers the thermal stress presented in the carbon fiber–epoxy laminate by reducing the matrix CTE. It has been found that the toughening caused by R-MWCNTs and O-MWCNTs can slightly improve the micro-cracks resistance of the laminates. On the contrary, the ordered Fe_3O_4/O-MWCNTs can reduce the crack density by 37.2%. From the previous results, it can be seen that Fe_3O_4/O-MWCNTs can reduce the CTE of the epoxy matrix more effectively than R-MWCNTs, and O-MWCNTs.

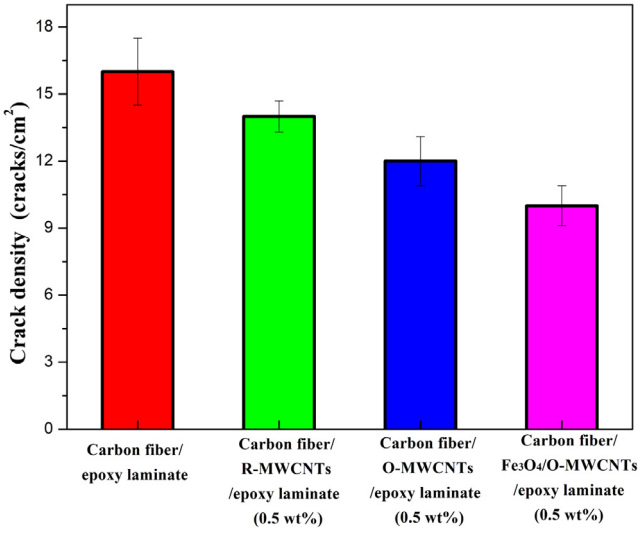

Fig. 9. Average crack densities of the various systems.

According to the above results, the mechanism of CNTs modifiers on the cryogenic toughening and micro-cracks resistance behaviors of modified CF/EP laminates under cryogenic thermal cycling was shown in Fig. 10. Because of the huge mismatch of CTE between the carbon fiber and the epoxy matrix, thermal stress could be generated in the CF/EP laminates when the laminates were exposed to temperature cycling. The micro-cracks propagate mostly through the interfacial zone between the carbon fiber and the epoxy matrix, as schematically demonstrated in Fig. 10a. This is due to poor interfacial interaction between the carbon fiber and the epoxy matrix. However, the micro-cracks propagation of CNTs modified CF/EP laminate is quite different from that of neat epoxy system. Carbon fibers were covered with the epoxy resin filled with CNTs and the micro-cracks propagated through the matrix (Fig. 10b–d). Because the R-MWCNTs have a lower CTE than epoxy, and the interface between R-MWCNTs and epoxy matrix is weak, the micro-cracks deflect toward the interface between the R-MWCNTs (Fig. 10b). This behavior can be explained by the crack deflection [44], in which the deflection toughening arises whenever the interaction between the crack front and the minor phase produces a non-planar crack. In the absence of crack deflection, a crack can propagate unimpededly through the matrix catastrophically when it encounters the fibers. This results in no toughening because little energy is dissipated during the crack propagation. When the crack deflection occurs, the crack twists from its initial propagation direction and circumvents the fillers without penetrating them. This produces an increase in the total surface area, leading to a higher energy absorption or an enhanced fracture toughness [44–46]. In our system, the non-planar crack arises from the existence of weakened interfaces between R-MWCNTs and epoxy matrix. As mentioned above, after oxidation, the —OH and —COOH groups were introduced on the surface of O-MWCNTs, which could form covalent bonding with epoxy matrix. The enhanced load transfer capability of the epoxy matrix shows that the micro-cracks zigzagged in the laminates (Fig. 10c) with

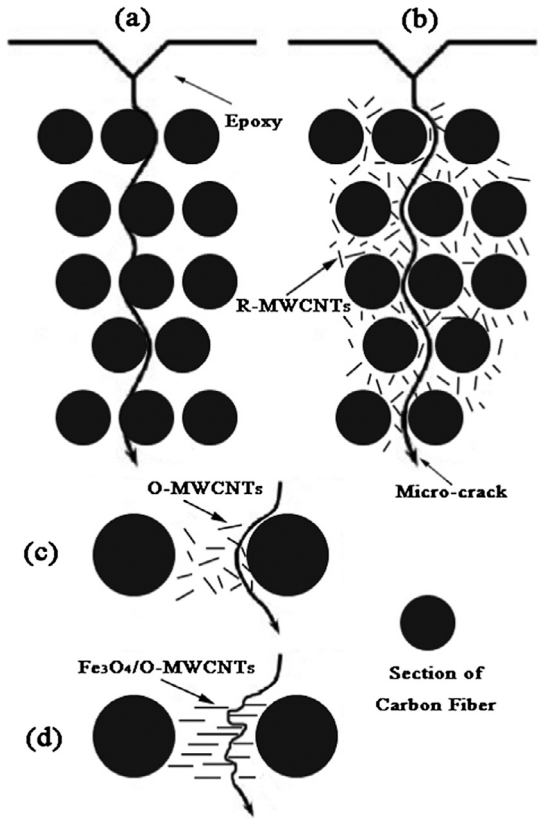

Fig. 10. Schematic diagram of the crack propagation and suppression behavior of CNTs modified CF/EP composites: (a) CF/EP laminate, (b) R-MWCNTs modified CF/EP laminate, (c) O-MWCNTs modified CF/EP laminate and (d) Fe_3O_4/O-MWCNTs modified CF/EP laminate. Arrows indicate the crack path.

enhanced mechanical properties. Induced by an external magnetic field, Fe_3O_4/O-MWCNTs were aligned orderly in epoxy matrix, which further improved the micro-cracks suppression between carbon fibers (Fig. 10d).

As a consequence, it can be suggested that the mechanism of micro-cracks resistance of CNTs modified CF/EP laminates under cryogenic thermal cycling is crack deflection, depending on its dispersity and interfacial interaction between CNTs and epoxy matrix.

4. Conclusions

Three types of multi-walled carbon nanotubes (MWCNTs) were used to modify epoxy and the mechanical properties, including the tensile strength and impact strength, of the modified epoxies at 77 K were studied systematically. The VARTM technique was adopted to prepare carbon fiber reinforced epoxy (CF/EP) laminates and the effect of MWCNTs on the micro-cracks resistance of the laminates was investigated. Results show that the presence of oriented Fe_3O_4/O-MWCNTs can increase the tensile strength, impact strength of epoxy resin and micro-cracks resistance at cryogenic temperature of carbon fiber reinforced epoxy composites and decrease the CTEs of the epoxy resin. The results indicated that it is feasible to orient the Fe_3O_4 modified O-MWCNTs in the epoxy matrix by an external magnetic field and the oriented Fe_3O_4/O-MWCNTs can further improve the micro-cracks resistance at cryogenic temperature of carbon fiber reinforced epoxy composites. These materials can be applied in cryogenic propellant tank for space shuttles and other applications such as sensing [47–50], functional materials [51–58], membrane or adsorbents for environmental remediation [59–61], and electromagnetic interference (EMI) shielding [62].

Acknowledgments

This project was financially supported by National Natural Science Foundation of China (No.U160425), Key Scientific and Technological Projects of Henan Province (No. 162102210052) and Public Welfare Technical Assistance Project of Zhejiang Province (2016C31031).

Appendix A. Supplementary material

Supplementary data associated with this article can be found, in the online version, at https://doi.org/10.1016/j.jcis.2018.01.087.

References

[1] S.A. Hawkins, H.Q. Yao, H.F. Wang, H.J. Sue, Carbon 115 (2017) 18–27.
[2] J.J. Jiang, X.M. Yao, C.M. Xu, Y. Su, L.C. Zhou, C. Deng, Compos. A Appl. Sci. Manuf. 95 (2017) 248–256.
[3] X.H. Cao, X.D. Wei, G.J. Li, C. Hu, K. Dai, J. Guo, et al., Polymer 112 (2017) 1–9.
[4] H.B. Gu, C. Ma, J.W. Gu, J. Guo, X.R. Yan, J.N. Huang, et al., J. Mater. Chem. C 4 (2016) 5890–5906.
[5] J. Guo, J. Long, D.W. Ding, Q. Wang, Y. Shan, A. Umar, et al., RSC Adv. 6 (2016) 21187–21192.
[6] H. Liu, M.Y. Dong, W.J. Huang, J.C. Gao, K. Dai, J. Guo, et al., J. Mater. Chem. C 5 (2017) 73–83.
[7] Q.S. Ma, Y.Z. Gu, M. Li, S.K. Wang, Z.G. Zhang, Appl. Surf. Sci. 379 (2016) 199–205.
[8] H.L. Ma, Z.M. Jia, K.T. Lau, X.F. Li, D. Hui, S.Q. Shi, Compos. B Eng. 110 (2017) 396–401.
[9] A. Montazeri, M. Chitsazzadeh, Mater. Des. 56 (2014) 500–508.
[10] J.S. Jang, J. Varischetti, G.W. Lee, J. Suhr, Compos. A Appl. Sci. Manuf. 42 (2011) 98–103.
[11] J.F. Timmerman, B.S. Hayes, J.C. Seferis, Compos. Sci. Technol. 62 (2002) 1249–1258.
[12] S.U. Khan, A. Munir, R. Hussain, J.K. Kim, Compos. Sci. Technol. 70 (2010) 2077–2085.
[13] M.G. Kim, J.S. Hong, S.G. Kang, C.G. Kim, Compos. A Appl. Sci. Manuf. 39 (2008) 647–654.
[14] T. Yokozeki, Y. Iwahori, S. Ishiwata, Compos. A Appl. Sci. Manuf. 38 (2007) 917–924.
[15] M. Nobelen, B.S. Hayes, J.C. Seferis, J. Appl. Polym. Sci. 90 (2003) 2268–2275.
[16] Y.X. He, L. Zhang, G.W. Chen, X.Y. Li, D.H. Yao, J.H. Lee, et al., Polym. Bull. 71 (2014) 2465–2485.
[17] X.Y. Yang, X.Y. Zhang, Y.F. Ma, Y. Huang, Y.S. Wang, Y.S. Chen, J. Mater. Chem. 323 (2009) 1006–1010.
[18] Y.X. He, G.W. Chen, L. Zhang, Y.F. Sang, C. Lu, D.H. Yao, et al., High Perform. Polym. 26 (2014) 922–934.
[19] A. Demira, A. Baykal, H. Sözeri, R. Topkaya, Synth. Met. 187 (2014) 75–80.
[20] M. Günay, A. Baykal, H. Sözeri, Structural, J. Supercond. Nov. Magn. 25 (2012) 2415–2420.
[21] M. Gunay, H. Kavas, A. Baykal, Mater. Res. Bull. 48 (2013) 1296–1303.
[22] S.Q. Song, H.X. Yang, R.C. Rao, H.D. Liu, A. Zhang, Appl. Catal. A 375 (2010) 265–271.
[23] Y.Q. Zhan, R. Zhao, Y.J. Lei, F.B. Meng, J.C. Zhong, X.B. Liu, J. Magn. Magn. Mater. 323 (2011) 1006–1010.
[24] V. Cleveland, J.P. Bingham, E.S. Kan, Sep. Purif. Technol. 133 (2014) 388–395.
[25] D.H. Xu, G.E. Luo, J.F. Yu, W.Y. Chen, C.C. Zhang, O.Y. Dong, et al., J. Alloy. Compd. 702 (2017) 499–508.
[26] M.B. Gholivand, M. Solgi, Anal. Biochem. 520 (2017) 1–8.
[27] S.W. Lu, W.K. Xu, X.H. Xiong, K.M. Ma, X.Q. Wang, J. Alloy. Compd. 606 (2014) 171–176.
[28] J. Guo, H.X. Song, H. Liu, C.J. Luo, Y.R. Ren, T. Ding, et al., J. Mater. Chem. C 5 (2017) 5334–5344.
[29] Y.X. He, Y.F. Sang, L. Zhang, D.H. Yao, K.B. Sun, Y.Q. Zhang, Plast. Rubber Compos. 43 (2014) 89–97.
[30] J. Kathi, K.Y. Rhee, J. Mater. Sci. 43 (2008) 33–37.
[31] D.W. Jiang, L.X. Xing, L. Liu, X. Yan, J. Guo, X. Zhang, et al., J. Mater. Chem. A 2 (2014) 18293–18303.
[32] D.W. Jiang, L.X. Xing, L. Liu, S.F. Sun, Q.B. Zhang, Z.J. Wu, et al., Compos. Sci. Technol. 117 (2015) 168–175.
[33] D.W. Jiang, L. Liu, J. Long, Y.D. Huang, Z.J. Wu, X.R. Yan, et al., Compos. Sci. Technol. 100 (2014) 158–165.
[34] X.H. Liu, F.J. Xu, K. Zhang, B.C. Wei, Z.Q. Gao, Y.P. Qiu, Compos. Sci. Technol. 145 (2017) 114–121.
[35] S.Y. Fu, X.Q. Feng, B. Lauke, Y.W. Mai, Compos. B Eng. 39 (2008) 933–961.
[36] X. Zhang, O. Alloul, Q.L. He, J.H. Zhu, M.J. Verde, Y.T. Li, et al., Polymer 54 (2013) 3594–3604.
[37] Z.H. Guo, T. Pereira, O. Choi, Y. Wang, H.T. Hahn, J. Mater. Chem. 16 (2006) 2800–2808.
[38] S.R. Wang, Z.Y. Liang, P. Gonnet, Y.H. Liao, B. Wang, C. Zhang, Adv. Funct. Mater. 17 (2007) 87–92.

[39] T. Ogasawara, S. Hanamitsu, T. Ogawa, S.Y. Moon, Y. Shimamura, Y. Inoue, Adv. Compos. Mater. 26 (2017) 157–168.
[40] Z. Kornain, A. Jalar, R. Rasid, S. Abdullah, Adv. Mater. Res. 97–101 (2010) 23–27.
[41] X.S. Zhang, L.W. Yang, H.T. Liu, M. Zu, RSC Adv. 7 (2017) 23334–23341.
[42] Q.P. Feng, Y.H. Deng, H.M. Xiao, Y. Liu, C.B. Qu, Y. Zhao, et al., Compos. Sci. Technol. 104 (2014) 59–65.
[43] J.W. Li, Z.X. Wu, C.J. Huang, L.F. Li, Compos. Sci. Technol. 104 (2014) 81–88.
[44] J.T. Han, K. Cho, Macromol. Mater. Eng. 290 (2005) 1184–1191.
[45] X.M. Chen, M. Zheng, C. Park, C.H. Ke, Small 9 (2013) 3345–3351.
[46] M.A. Rafiee, J. Rafiee, I. Srivastava, Z. Wang, H.H. Song, Z.Z. Yu, et al., Small 6 (2010) 179–183.
[47] Y. Li, B. Zhou, G. Zheng, X. Liu, T. Li, et al., J. Mater. Chem. C (2018), https://doi.org/10.1039/C7TC04959E. in press.
[48] H. Liu, Y. Li, K. Dai, G. Zheng, C. Liu, C. Shen, et al., J. Mater. Chem. C 4 (2016) 157–166.
[49] X. Guan, G. Zheng, K. Dai, C. Liu, X. Yan, C. Shen, Z. Guo, ACS Appl. Mater. Interf. 8 (2016) 14150–14159.
[50] H. Liu, W. Huang, X. Yang, K. Dai, G. Zheng, et al., J. Mater. Chem. C 4 (2016) 4459–4469.
[51] X. Wang, X. Liu, H. Yuan, H. Liu, C. Liu, et al., Mater. Des. 139 (2018) 372–379.
[52] M. Zhao, L. Meng, L. Ma, X. Yang, Y. Huang, J. Ryu, A. Shankar, T. Li, C. Yan, Z. Guo, Compos. Sci. Technol. 154 (2018) 28–36.
[53] Z. Wu, S. Gao, L. Chen, D. Jiang, Q. Shao, B. Zhang, et al., Macromol. Chem. Phys. 218 (2017) 1700357.
[54] K. Sun, P. Xie, Z. Wang, T. Su, Q. Shao, et al., Polymer 125 (2017) 50–57.
[55] C. Cheng, R. Fan, Z. Wang, Q. Shao, X. Guo, et al., Carbon 125 (2017) 103–112.
[56] J. Zhao, L. Wu, C. Zhan, Q. Shao, Z. Guo, L. Zhang, Polymer 133 (2017) 272–287.
[57] C. Wang, M. Zhao, J. Li, J. Yu, S. Sun, et al., Polymer 131 (2017) 263–271.
[58] S. Zhao, G. Li, H. Liu, K. Dai, G. Zheng, et al., Adv. Mater. Interfaces 4 (2017) 1700265.
[59] Y. Ma, L. Lyu, Y. Guo, Y. Fu, et al., Polymer 128 (2017) 12–23.
[60] J. Huang, Y. Cao, Q. Shao, X. Peng, Z. Guo, Ind. Eng. Chem. Res. 56 (2017) 10689–10701.
[61] X. Cheng, Z. Wang, X. Jiang, T. Li, C. Lau, et al., Progress, Mater. Sci. 92 (2018) 258–283.
[62] K. Zhang, G. Li, L. Feng, N. Wang, J. Guo, et al., J. Mater. Chem. C 5 (2017) 9359–9369.